Surface states and annihilation characteristics of positrons trapped at the (100) and (111) surfaces of silicon

N. G. Fazleev,[1,2] J. L. Fry,[1] and A. H. Weiss[1]
[1]*Department of Physics, Box 19059, University of Texas at Arlington, Arlington, Texas 76019-0059, USA*
[2]*Department of Physics, Kazan State University, Kazan 420008, Russian Federation*
(Received 21 January 2004; revised manuscript received 26 July 2004; published 13 October 2004)

Recent studies of Si(100) and Si(111) using positron annihilation induced Auger-electron spectroscopy (PAES) reveal that experimental annihilation probabilities of surface trapped positrons with relevant Si core-level electrons differ significantly for two faces of clean Si, an elemental semiconductor. These experimental results are investigated theoretically by performing calculations of the "image-potential" positron surface states and annihilation characteristics of the surface trapped positrons with relevant Si core-level electrons for the ideally terminated, nonreconstructed and reconstructed Si(100)-(2×1) and Si(111)-(7×7) surfaces. Computed positron surface binding energies demonstrate their sensitivity to the specific atomic structure of the topmost layers of surfaces, and, when compared to positron work functions, the stability of positron surface states on all studied Si(100) and Si(111) surfaces. The positron surface state wave function was found to be localized in a potential well on the vacuum side at both nonreconstructed semiconductor surfaces. The (2×1) reconstruction of the Si(100) surface causes the positron surface state wave function to extend into the lattice in the regions where atoms are displaced away from their ideal terminated positions. A comparison of theoretical and experimental positron surface binding energies for Si(100) shows that the best agreement is achieved when the reconstructed Si(100)-(2×1) surface is described within the asymmetric dimer model. Calculations indicate that the positron surface state wave function is localized in all three dimensions in the corner hole regions of the reconstructed Si(111)-(7×7) surface. This localization provides an explanation for previous experiments that failed to show the anisotropy in the electron-positron pair momentum density distribution expected for a positron surface state delocalized in the plane of the surface. Positron annihilation characteristics are calculated for each surface and compared with experimental positron spectroscopy data. These calculations reveal strong dependence of positron annihilation characteristics on the crystal face of clean Si in contrast to the much smaller face dependence found on clean metal surfaces. Annihilation probabilities of surface trapped positrons with Si *2s*- and *2p*-core-level electrons are found to be significantly smaller for the reconstructed Si(111)-(7×7) surface when compared with the results for the reconstructed Si(100)-(2×1) surface, in agreement with experimental PAES data. These results indicate that PAES intensities, which are proportional to core annihilation probabilities, are sensitive to the crystal face and surface structure of an elemental semiconductor.

DOI: 10.1103/PhysRevB.70.165309 PACS number(s): 78.70.Bj, 71.60.+z, 68.47.Fg, 68.35.Bs

I. INTRODUCTION

Spatially extended "image-potential" electronic states near the surfaces of conductors have been intensely studied both theoretically and experimentally due to their role in surface phenomena and interest in quantum states of reduced dimensionality.[1,2] Like electrons, positrons can have surface-bound states localized in the region of the vacuum-medium interface.[3,4] These surface states are the consequence of the interplay between repulsion from the surface ionic cores and electron–positron correlations just outside the surface resulting in an attractive interaction. Their properties are critically dependent on the nature of the short-range "correlation well" in the vicinity of the surface atoms. Unlike the electron case, the "image-potential" surface states for positrons typically have lower energies than the bulk positron states, and these states form a trap for positrons that encounter the surface. The existence of positron surface states on metal and semiconductor surfaces has been demonstrated by the observation that positrons could be thermally desorbed from clean surfaces at elevated temperatures as positronium.[5–8]

Positron surface states and annihilation characteristics of low energy positrons trapped at metal and semiconductor surfaces are of interest because of the possibilities of using positrons in the development of new probes of surfaces, thin films, and nanostructures. In addition, the positron annihilation characteristics provide a means of studying fundamental questions pertaining to the nature of "image-potential" positron surface states, which are examples of "quasi-two-dimensional" states of distinguishable, light, quantum particles.

Experimental studies of the nature and localization of the positron bound states at metal surfaces, both clean and adsorbate-covered, have been performed using a surface characterization technique, positron annihilation induced Auger electron spectroscopy (PAES).[9–16] Under the conditions used in PAES experiments most of the low energy positrons implanted into the sample under study diffuse back to the vacuum–solid interface where on the order of half are trapped into a surface state. A certain fraction of the surface trapped positrons annihilates with neighboring core-level electrons, creating core-hole excitations that give rise to

 ©2004 The American Physical Society

Auger-electron emission. The intensities of the measured positron annihilation induced Auger signals are directly related to the core annihilation probabilities $p_{n,l}$, the fractions of positrons trapped in the surface state annihilating with electrons from different core shells with principal and angular momentum numbers n and l.[9,17]

Recently, the PAES technique has been applied to study the positron surface states and the positron annihilation induced Auger spectra from two different faces of an elemental semiconductor,[17] Si(100)-(2×1) and Si(111)-(7×7). PAES signals obtained from both semiconductor surfaces display a strong Auger peak in the measured energy range corresponding to the $L_{2,3}VV$ Auger transition for Si (see Figs. 1 and 2 from Ref. 17). Several important facts can be deduced from the experimental PAES data taken from the Si(100) and Si(111) surfaces.[17]

First, unlike different surfaces of transition metals,[18–24] the PAES signals from the two Si surfaces are significantly different. The experimental probability of annihilation of the surface trapped positrons that results in a Si $2p$ core hole calculated from the PAES intensities has been found to be: $2.01\% \pm 0.02\%$ and $0.65\% \pm 0.01\%$ for the reconstructed Si(100)-(2×1) and Si(111)-(7×7) surfaces, respectively.[17] In contrast the clean transition metal surfaces show little variation of positron annihilation characteristics for different surfaces of the same transition metal.[18–24] Second, the PAES intensities for Si are significantly smaller than the corresponding Auger signal intensities at transition metal surfaces.[18] Third, the experimental probabilities of annihilation of the surface trapped positrons with Si core-level electrons calculated from the PAES intensities for both Si surfaces are significantly smaller compared to the ones obtained for the Cu(100) and Cu(111) surfaces.[16,17]

In this paper we present the results of theoretical studies of positron surface states and positron annihilation characteristics at the (100) and (111) surfaces of Si with different reconstructions. Such studies are indispensable for interpreting PAES experiments and clarifying the formation, stability, and localization of positron surface states at semiconductor surfaces. They provide surface structure dependence of probabilities of annihilation of the surface trapped positrons with Si core-level electrons.

The remainder of this paper is organized as follows. Section II details the construction of a potential for a positron at a semiconductor surface. Section III presents the results of calculations of positron surface states at the ideally terminated, non-reconstructed and reconstructed Si(100)-(2×1) and Si(111)-(7×7) surfaces. Positron annihilation characteristics are reported in Sec. IV. The computed positron surface state annihilation characteristics are compared with experimental PAES data and with positron annihilation characteristics obtained for bulk Si and Cu, and for the clean (100) and (111) surfaces of Cu. Annihilation probabilities of the surface trapped positrons with relevant Si core-level electrons are found to be significantly smaller for the reconstructed Si(111)-(7×7) surface when compared with the results for the reconstructed Si(100)-(2×1) surface, in agreement with experimental data. Conclusions are summarized in Sec. V.

II. POSITRON POTENTIAL AT A SEMICONDUCTOR SURFACE

We perform calculations of positron surface and bulk states in the present paper using the modified superimposed-atom method to account for discrete-lattice effects.[4,22] Earlier calculations based on this method have been successful in analyzing the formation and localization of the positron surface states at transition metal surfaces.[19–22] This approach is computationally efficient and makes a study of reconstructed surfaces possible using the same techniques as for non-reconstructed surfaces.

We describe the positron potential $V^+(\boldsymbol{r})$ at a semiconductor as an electrostatic Hartree (Coulomb) potential $V_H(\boldsymbol{r})$, and a correlation potential $V_{\text{corr}}(\boldsymbol{r})$:

$$V^+(\boldsymbol{r}) = V_H(\boldsymbol{r}) + V_{\text{corr}}(\boldsymbol{r}). \tag{1}$$

The Hartree potential $V_H(\boldsymbol{r})$ is constructed as a superposition of the atomic Coulomb potentials $V^{at}_{\text{Coul}}(|\boldsymbol{r}-\boldsymbol{R}|)$ from all the atoms located within a predetermined radius of the evaluation point, where $\boldsymbol{R}$ defines the positions of the host nuclei.

Atomic calculations for the Si atom are performed within the local-spin-density approximation[25] using the exchange-correlation functional and atomic configurations from Refs. 26 and 27, respectively. The Schrödinger equation is solved self-consistently for each bound electron state of the Si atom. The criterion for convergence is that the change in the energy of each bound electron from one iteration to the next is less than 10^{-8} H. The resulting wave functions are then used to find the electron densities and corresponding atomic potentials via Poisson's equation. The crystal structure and the lattice constant for bulk silicon are taken from Ref. 28. The resulting total electron density $n_-(\boldsymbol{r})$ at the semiconductor surface is approximated by the superposition of the calculated atomic electron densities:

$$n_-(\boldsymbol{r}) = \sum_{\boldsymbol{R}} n^{at}_-(|\boldsymbol{r}-\boldsymbol{R}|), \tag{2}$$

where $\boldsymbol{R}$ summation takes place over the positions of the nuclei. We note that in bulk semiconductors, the superimposed electron density provides a good estimate of the electron density in the interstitial region (the region in which the positron wave function is mainly localized in the bulk).[29] The resulting Hartree potential $V_H(\boldsymbol{r})$ is constructed in a similar way:

$$V_H(\boldsymbol{r}) = \sum_{\boldsymbol{R}} V^{at}_{\text{Coul}}(|\boldsymbol{r}-\boldsymbol{R}|). \tag{3}$$

The positron-electron correlation potential $V_{\text{corr}}(\boldsymbol{r})$ reflects the response of the electron charge density to the presence of the positron by taking into account many body effects. As in the case of metal surfaces, in constructing $V_{\text{corr}}(\boldsymbol{r})$ at a semiconductor surface, we exploit the fact that the electron density is much higher near the surface of a semiconductor than it is in the vacuum, far from the surface. The correlation component of the positron potential $V^+(\boldsymbol{r})$ in the region where the electron density is high (deep inside) is well described using the local density approximation (LDA). The image-type potential is used to describe the correlation com-

ponent of $V^{+}(\boldsymbol{r})$ in the region far outside the semiconductor surface, where the electron density is assumed to be zero. We then divide the space into two regions, namely, the bulk and image potential regions, where the two models are applied. The boundary between these regions is chosen to pass through the crossover point of the bulk and image-type potentials, located immediately outside the surface.

In the LDA $V_{\text{corr}}(\boldsymbol{r})$ is obtained at a given position by considering the positron to be embedded in a homogeneous electron gas with an electron density n_{-} corresponding to the electron density at that particular point, i.e.,

$$V_{\text{corr}}(\boldsymbol{r}) = V_{\text{corr}}^{\text{LDA}}(\boldsymbol{r};n_{-}) = V_{\text{corr}}^{\text{EG}}(n_{-})[f(n_{-},\varepsilon_g)]^{1/3}, \tag{4}$$

where $V_{\text{corr}}^{\text{EG}}(n_{-})$ is the correlation energy for a positron in a homogeneous electron gas[30] of density n_{-}. When constructing $V_{\text{corr}}^{\text{LDA}}(\boldsymbol{r};n_{-})$ we take into consideration that valence electrons in semiconductors, due to the existence of a band gap, do not respond to an external perturbation as effectively as conduction electrons in metals. As a result, the screening of a positron by valence electrons in semiconductors is not perfect. In addition, the positron is much lighter than the ions, which have no time to rearrange in response to the instantaneous position of the positron. Consequently, the asymptotic form of the long-range Coulomb potential due to the positron should be proportional to $1/\varepsilon_{\infty}r$, where ε_{∞} is the high-frequency dielectric constant of the medium, and the screening cloud $\Delta n_{-}(r)$, induced by the positron in the medium characterized by the dielectric constant ε_{∞}, should satisfy the following sum rule for the induced electron density:

$$\int_{0}^{\infty} \Delta n_{-}(r) 4\pi r^2 dr = \left(1 - \frac{1}{\varepsilon_{\infty}}\right). \tag{5a}$$

The electron density $n_{-}(r)$ screening the positron at the origin $(r=0)$ satisfies the cusp condition:

$$\left.\frac{\partial n_{-}(r)}{\partial r}\right|_{r=0} = -n_{-}(0). \tag{5b}$$

The function $f(n_{-},\varepsilon_g)$ in Eq. (4) is a reduction factor which accounts for the diminished screening response of semiconductors to charged particles due to the existence of a band gap, in comparison to metals for which $f=1$. The "gap parameter" ε_g describes the effect of the band gap on the electron-positron correlation, and is related to the widths of the band gap and the valence band as $\varepsilon_g = E_g/E_F$, where E_F is the Fermi energy. According to calculations of Brandt and Reinheimer[31] of a reduction factor f for a set of r_s and ε_g values, a reasonable fit to their numerical data, obtained from screening calculations for point charges in a model semiconductor, can be obtained using the following interpolation formula:

$$f(n_{-},\varepsilon_g) = 1 - \frac{0.37\varepsilon_g}{1 + 0.18 r_s}, \tag{6}$$

with $r_S = (3/4\pi n_{-})^{1/3}$. The parameter ε_g was determined in Ref. 31 in terms of the high-frequency dielectric constant ε_{∞} of the semiconductor under consideration. In the present work we treat ε_g as a parameter, and use the value, $\varepsilon_g = 0.2$, which was shown to reproduce well the experimental annihilation rates for delocalized positron states in several IV– and III–V-type semiconductors.[32] In this work we use the parametrized version for the electron-positron correlation energy per electron for a positron in a homogeneous electron gas proposed by Boronski and Nieminen.[33]

The positron-electron correlation potential outside the semiconductor surface described by the image-type potential is constructed to have the same corrugations as the total electron density $n_{-}(\boldsymbol{r})$:

$$V_{\text{image}}(\boldsymbol{r}) = -\frac{e^2}{16\pi\varepsilon_0}\frac{(\varepsilon_{\infty}-1)}{(\varepsilon_{\infty}+1)}\frac{1}{[Z_{\text{eff}}[n_{-}(\boldsymbol{r})] - Z_0]}, \tag{7}$$

where e is the charge of a positron, ε_0 is the vacuum permittivity, ε_{∞} is the high-frequency dielectric constant of the semiconductor, $Z_{\text{eff}}[n_{-}(\boldsymbol{r})]$ is the effective distance from the surface, represented as a function of the total electron density at the surface, $n_{-}(\boldsymbol{r})$, and Z_0 defines the effective image-plane position on the vacuum side of the top layer of atoms. The joining of the image-type potential to the local density correlation potential is done by taking $V_{\text{corr}}(\boldsymbol{r})$ to be the larger of the two at each point outside the surface.

The presence of the occupied electron surface states and the charge imbalance resulting from the termination of bulk semiconductor, affect the electron distribution functions at the surface. To account for these charge rearrangement effects on the electron distribution functions and the positron potential at the Si(100) and Si(111) surfaces within the superimposed-atom method, calculations of the positron surface state are performed with the addition of a ramp potential $V_{\text{surf}}(z)$ to the expression for the total positron potential $V^{+}(\boldsymbol{r})$:

$$V_{\text{surf}}(z) = \begin{cases} \Delta V, & z < z_1, \\ \Delta V(z - z_2)/(z_1 - z_2), & z_1 < z_2 \\ 0, & z > z_2. \end{cases} \tag{8}$$

The coordinates z_1 and z_2 define the spatial extent of the surface charge arrangement area. The height of the ramp potential ΔV is adjusted for the surface to provide the potential felt by the positron at the semiconductor surface that gives the proper positron work function for each surface.

III. POSITRON SURFACE STATES

The positron potential and the electron density are defined at the node points of the three-dimensional mesh forming a polyhedron that, due to symmetry considerations, is capable of describing the potential and wave functions at the entire surface. The positron is assumed to be in the ground state and delocalized in the XY plane of the semiconductor surface, and to have a crystal momentum in this plane of $\mathbf{k}=0$. The outermost plane of Si atoms is taken to reside at $Z=0$. The extent of the positron surface state wave function into the vacuum outside the semiconductor surface and inside the semiconductor lattice is determined by the computational cell boundaries in the direction perpendicular to the surface

(Z direction). These boundaries are chosen to be far (up to ten lattice parameters) from the topmost layer of Si atoms.

A discretized version of the three-dimensional Schrödinger equation for the positron eigenenergy and the positron surface state wave function:

$$-\frac{\hbar^2}{2m}\nabla^2\psi_i^+(\boldsymbol{r})+[V_H(\boldsymbol{r})+V_{\rm corr}(\boldsymbol{r})+V_{\rm surf}(z)]\psi_i^+(\boldsymbol{r})=E_i\psi_i^+(\boldsymbol{r}), \tag{9}$$

is solved numerically using a finite difference relaxation technique.[4,34] The positron surface state energy and the positron surface state wave function are found through iteratively solving for the energy, and then correcting the wave function based on the energy, the positron potential, and the values of the wave function at the surrounding mesh points. The computer code used in calculations is discussed in Ref. 23. Delocalized states in the plane of the semiconductor surface (the XY plane) are obtained by using boundary conditions which continue the wave function through the polyhedron surfaces (in the X and Y directions). The image plane position Z_0 is determined from Lang–Kohn theory.[35] The high frequency dielectric constant ε_∞ equals 12.0 for Si.[36]

Initially we perform calculations of the energy of the lowest lying positron bulk state $E_\infty^{\rm theor}$ relative to the vacuum zero level in bulk Si terminated by the (100) and (111) surfaces to determine the height ΔV of the ramp potential for all nonreconstructed and reconstructed Si surfaces that is used later in the positron surface state calculations (the value of ΔV for each surface is determined by the condition that $E_\infty^{\rm theor}$ equals $-\Phi_+^{\rm exper}$). To avoid inconsistencies in calculations of the positron work function $\Phi_+^{\rm theor}$ and the positron binding energy $E_b^{\rm theor}$, associated with the use of different computational schemes, potentials, and different energy reference levels, we perform calculations of the energy of the lowest lying positron bulk state within the modified superimposed-atom method employing the same total positron potential and the same energy reference level (the vacuum zero) that are used in positron surface state calculations. The lowest lying positron bulk state energies $E_\infty^{\rm theor}$ in bulk Si terminated by the (100) and (111) surfaces are found by solving the three-dimensional Schrödinger equation numerically using the finite difference relaxation technique.[4,34] Atomic structures of the non-reconstructed and reconstructed Si(100)-(2×1) and Si(111)-(7×7) surfaces used in numerical calculations are discussed later. Similar to the positron surface state calculations, the electron density and the positron potential are calculated at the node points of a three-dimensional mesh. It is assumed that the positron wave function deep inside the bulk Si approaches periodicity in the Z direction with a period of one lattice parameter and that the positron wave function with $\mathbf{k}=0$ is the lowest Bloch state. The density of mesh points in the bulk state calculations is chosen to be similar or larger than the ones used in the surface state calculations. The results for $\Phi_+^{\rm exper}$, $E_\infty^{\rm theor}$ and ΔV obtained for bulk Si terminated by the (100) and (111) surfaces are displayed in Table I.

TABLE I. Experimental positron work function Φ_+, theoretical ground state energy for the bulk E_∞, and the ramp potential ΔV for the clean nonreconstructed Si(100) and Si(111) surfaces, the reconstructed Si(100)-(2×1) surfaces described within symmetric and asymmetric dimer models, and the reconstructed Si(111)-(7×7) surface described within the DAS model.

System	Φ_+ (eV) Experiment	E_∞ (eV) Theory	ΔV (eV)
Nonreconstructed Si(100)	0.3[a,b]	−0.30	0.781
Reconstructed Si(100)-(2×1) symmetric dimer model	0.3[a,b]	−0.30	0.782
Reconstructed Si(100)-(2×1) asymmetric dimer model	0.3[a,b]	−0.30	0.931
Nonreconstructed Si(111)	0[a,b]	0.00	1.018
Reconstructed Si(111)-(7×7) DAS model	0[a,b]	0.00	1.061

[a]Reference 37.
[b]Reference 40.

A. Positrons at the non-reconstructed Si(100) and Si(111) surfaces

The initial calculations of the positron surface state wave function and positron surface binding energy are performed for the clean non-reconstructed Si(100) and Si(111) surfaces. The crystal structure and the lattice constant for Si are taken from Ref. 28. The non-reconstructed (100) and (111) surfaces of Si in the diamond cubic structure have a square unit cell, and their surface atoms are second nearest neighbors. The outermost plane of Si atoms is taken to reside at $Z=0$. The effective image-plane position Z_0 is determined to be 2.88 a.u. for Si(100) and 3.82 a.u. for Si(111) from the top layer of atoms along a reference line. The height of the ramp potential ΔV is found to be equal to 0.78 and 1.02 eV for the Si(100) and Si(111) surfaces, respectively (see Table I) from a comparison of the calculated $E_\infty^{\rm theor}$ in bulk Si terminated by the (100) and (111) surfaces and the experimental $\Phi_+^{\rm exper}$ determined for both surfaces.[37]

Tight-binding calculations[38,39] indicate that the non-reconstructed Si(100) surface gives rise to two bands of electron surface states in the energy gap between the valence and conduction bands. One band (the dangling bond band) has its electron density localized about a line through and normal to the surface atoms, with a node on the atoms. The other band (the bridge bond band) has its charge density located around a line through a row of surface atoms and pointing toward neighboring surface atoms in the [110] direction. It follows from tight-binding calculations of the surface electronic structure[38,39] that the non-reconstructed Si(111) surface gives rise to a highly localized surface state band in the fundamental gap. In addition, both non-reconstructed surfaces give rise to electron "back-bond" surface states in one of the gaps of the projected valence band with corresponding charge density localized between the top and the second layers. Accordingly, the position of the start of the ramp potential, z_1, is taken to coincide with the plane of the second layer of Si atoms [z_1 is equal to −2.565 and −1.482 a.u. for the Si(100)

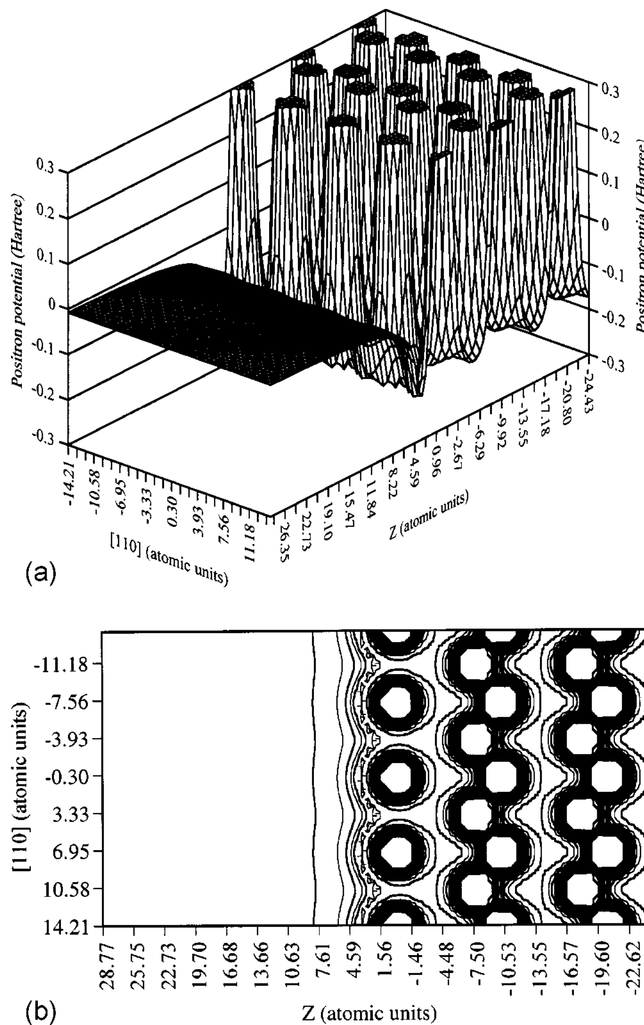

FIG. 1. Calculated potential for a positron at the clean non-reconstructed Si(100) surface. A: 3D plot (viewed from the vacuum side) for $Y^*=0$. B: Contour plot in the X^*-Z plane for $Y^*=0$ displayed with the vacuum side on the left. Contours are separated by 0.0425 Hartree.

and Si(111) surfaces, respectively] and the end of the ramp potential, z_2, is set at distance $d/2$ above the plane of the top atoms, where d is the interlayer spacing.

The plots of the positron potential for the value $Y^*=0$ for the Si(100) and Si(111) surfaces are presented in Figs. 1 and 2, respectively. Note, in all plots in the paper the X^* and Y^* axes are taken along the [110] and $[\bar{1}10]$ directions, respectively. It may be seen in these plots that, similar to the case of transition metal surfaces, the positron potential for the non-reconstructed (100) and (111) surfaces of Si contains small corrugations on the vacuum side of the topmost layer of Si atoms. The corresponding positron surface state wave functions for the value $Y^*=0$ for the non-reconstructed Si(100) and Si(111) surfaces are shown in Figs. 3 and 4, respectively. The positron is trapped mainly in the "*quasi-one-dimensional*" image-correlation well just outside the clean non-reconstructed surfaces of Si. The "*quasi-2d*" positron surface state wave function has its maximum about 2.32 and 3.07 a.u. outside the topmost layer of atoms for Si(100) and Si(111), respectively, and experiences a rapid drop with distance into the semiconductor lattice and overlaps very little with atoms of the second layer and beyond. Similar behavior of the positron surface state wave function has been observed at the clean transition metal surfaces. The computed binding energies of a positron trapped at the non-reconstructed (100) and (111) surfaces of Si converge to $E_b^{\text{theor}}=2.53$ eV and $E_b^{\text{theor}}=3.20$ eV with respect to vacuum compared to the experimental values of $E_b^{\text{exper}}=2.06(7)$ eV and $E_b^{\text{exper}}=2.69$ eV, respectively.[5,40] For both the non-reconstructed Si(100) and Si(111) surfaces the binding energy of the positron is larger than the corresponding positron work function. Thus, the calculated positron surface states are the ground states for both surfaces. The binding energy E_b values calculated for the Si(100) and Si(111) surfaces are comparable to the ones obtained for corresponding surfaces of Cu. As with their transition metal counterparts, E_b^{theor} is larger for the Si(111) surface as compared to the Si(100) surface due to the Si(111) surface's higher atomic surface density and its correspondingly larger surface electron density.

B. Positrons at the reconstructed Si(100)-(2×1) surface

At room temperature, the (100)-oriented surface of Si exhibits a (2×1) reconstruction in which the atoms of adjacent atom rows along the $[\bar{1}10]$ direction lean toward each other forming dimers.[41] Though the Si(100)-(2×1) surface has been extensively studied, there is still a question under debate as to whether the dimers are symmetric or asymmetric.[41–47] According to the symmetric dimer model[41–45] for the (2×1) reconstruction, adjacent rows of surface atoms spontaneously move in the surface plane to join via their bridge bond and form double rows along the $[\bar{1}10]$ direction. It is assumed that the reconstruction keeps the bond lengths the same as in the bulk but distorts bond angles. Thus, the surface atomic displacements have both a horizontal (1.4178 a.u.) and a vertical (0.4348 a.u.) component. In the simplest geometry of the asymmetric dimer model for the (2×1) reconstruction of the Si(100) surface,[46,47] the only allowed atomic displacements in the surface layer are those that keep all bond lengths equal to their bulk value. With this constraint, the minimization of the total energy leads to the following displacements from the ideal unrelaxed positions of Si atoms of the dimer: $\Delta x_1^*=+0.8696$ a.u., $\Delta z_1=-0.1512$ a.u., $\Delta x_2^*=-2.0416$ a.u., $\Delta z_2=-1.0019$ a.u. In a more elaborate asymmetric dimer model, further relaxations up to the fifth layer from the surface are included, and, in the most stable geometry, all bond lengths at the surface remain within 2% of their bulk value.[46,47]

Calculations of the positron surface states are performed for the reconstructed Si(100)-(2×1) surface described by both models: (a) the symmetric dimer model, and (b) the asymmetric dimer model including relaxations up to the fifth layer from the surface. The positions of the lower lying Si atoms are taken to correspond to their positions for the ideal Si lattice.

These calculations are performed with values for ΔV of 0.78 and 0.93 eV for the symmetric and asymmetric dimer

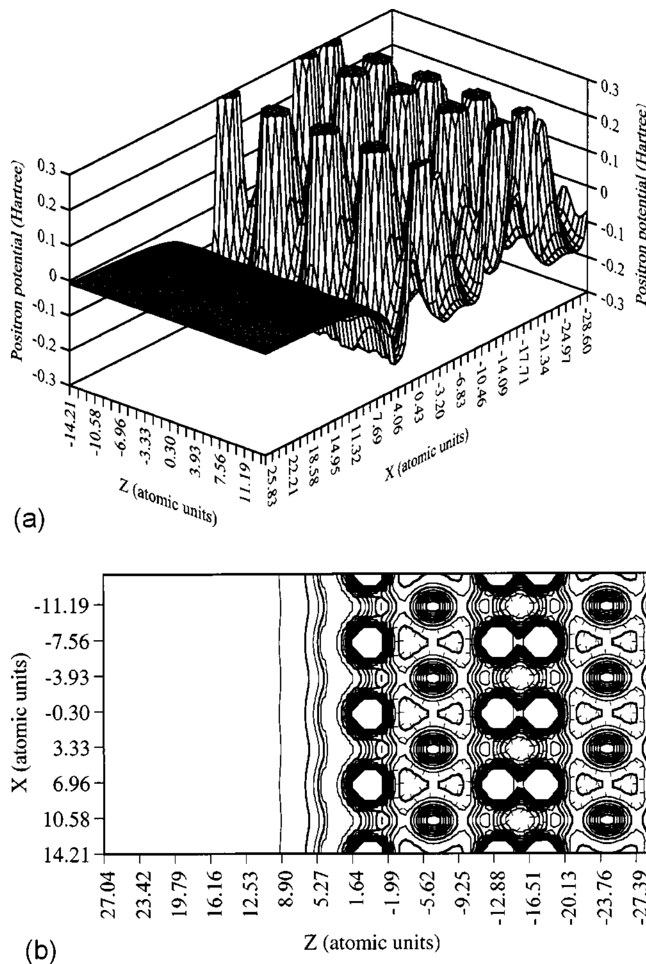

FIG. 2. Calculated potential for a positron at the clean non-reconstructed Si(111) surface. A: 3D plot (viewed from the vacuum side) for $Y=0$. B: Contour plot in the $X-Z$ plane for $Y=0$ displayed with the vacuum on the left. Contours are separated by 0.04 Hartree.

models, respectively (see Table I). These values provide the best agreement of $-E_{\infty}^{\text{theor}}$, computed for the two models of the reconstructed Si(100)-(2×1) surface, with the experimental positron work function Φ_{+}^{exper}. As it follows from the surface electronic structure calculations and core-level spectroscopy studies of the reconstructed Si(100)-(2×1) surface the reconstruction-induced rearrangements of electronic charge take place within the dimers and the layers beneath.[44,46,47] However, the amount of charge transferred rapidly decays from one layer to the next one with increasing depth into the bulk.[47] This provides a justification for a choice of the positioning of the start of the ramp potential, z_1, in the plane of the second layer of Si atoms beneath the dimers and of the end of the ramp potential, z_2, in the vacuum at $d/2$.

Plots of the positron potential and the surface state wave function are presented in Figs. 5–8. The positron potential for the reconstructed Si(100)-(2×1) surface (see Figs. 5 and 7) exhibits deep corrugations extending through the topmost layer into the lattice in the regions where atoms are displaced from their ideal positions due to the reconstruction. These corrugations affect the "*quasi-1d*" potential well responsible for localization of the positron on the vacuum side of the surface and shift its minima closer to the topmost layer of Si atoms than in the case of the non-reconstructed Si surface. Comparison of the plots in Figs. 3, 6, and 8 shows that the reconstruction of the Si(100) surface changes the localization and extent of the positron surface state wave function at the surface. The maximum of the positron surface state wave function at the reconstructed Si(100)-(2×1) surface described within the symmetric dimer model is significantly shifted toward the topmost layer of Si atoms, compared to the case of the unreconstructed Si(100) surface, and is located on the vacuum side about 0.333 a.u. outside the topmost layer of Si atoms. In the case of asymmetric dimers, the maximum of the positron surface state wave function is located about −0.438 a.u. below the outermost plane of Si atoms. Comparison of Figs. 3, 6, and 8 also shows that penetration of the positron surface state wave function, while still highly localized at the surface, into the Si lattice increases with reconstruction, and the penetration is the greatest in the case of the reconstructed Si(100)-(2×1) surface described within the asymmetric dimer model.

The computed binding energies of a positron trapped at the reconstructed Si(100)-(2×1) surface described within the symmetric and asymmetric dimer models converge to $E_b^{\text{theor}}=2.12$ and $E_b^{\text{theor}}=2.06$ eV, respectively. Comparison of the computed values with $E_b^{\text{exper}}=2.06(7)$ eV (Ref. 5) shows that the best agreement between theory and experiment is achieved when the reconstructed Si(100)-(2×1) surface is described within the asymmetric dimer model. Since the binding energy of the positron at the reconstructed Si(100) -(2×1) surface is larger than the corresponding positron work function the calculated positron surface state is the ground state for this reconstructed surface.

The computed values for E_b for the Si(100) surface are found to be smaller than the binding energies for the positrons trapped at the Cu(100) and Cu(111) surfaces, 2.77(5) and 2.80(5) eV, respectively,[15,16,18] reflecting the difference in the depth of the correlation well. The shallower well at the Si surface is a result in part of the lower total electron density in Si as compared to the transition metal, differences in electron-positron correlations in the transition metal and the elemental semiconductor, and to a change in the position of the image surface due to the (2×1) reconstruction of the Si(100) surface.

The extent to which the positron surface state wave function penetrates into the bulk can be understood qualitatively in terms of the energy difference between the surface and bulk states, $\Delta E=|E_b|-|\Phi_+|$, i.e., the larger the value of ΔE the less the surface state wave function penetrates into the bulk. This difference is larger for the (100) and (111) surfaces of Cu ($\Delta E=3.07$ and $\Delta E=3.15$ eV, respectively)[23] when compared to ΔE found for the non-reconstructed and reconstructed Si(100)-(2×1) surfaces described within the symmetric and asymmetric dimer models ($\Delta E=2.23$ eV, $\Delta E=1.82$ eV, and $\Delta E=1.76$ eV, respectively). As a result, the positron surface-bound-state wave function at the Si(100) surface penetrates further into the bulk semiconductor than the one found for transition-metal surfaces.[18,22,23] The results

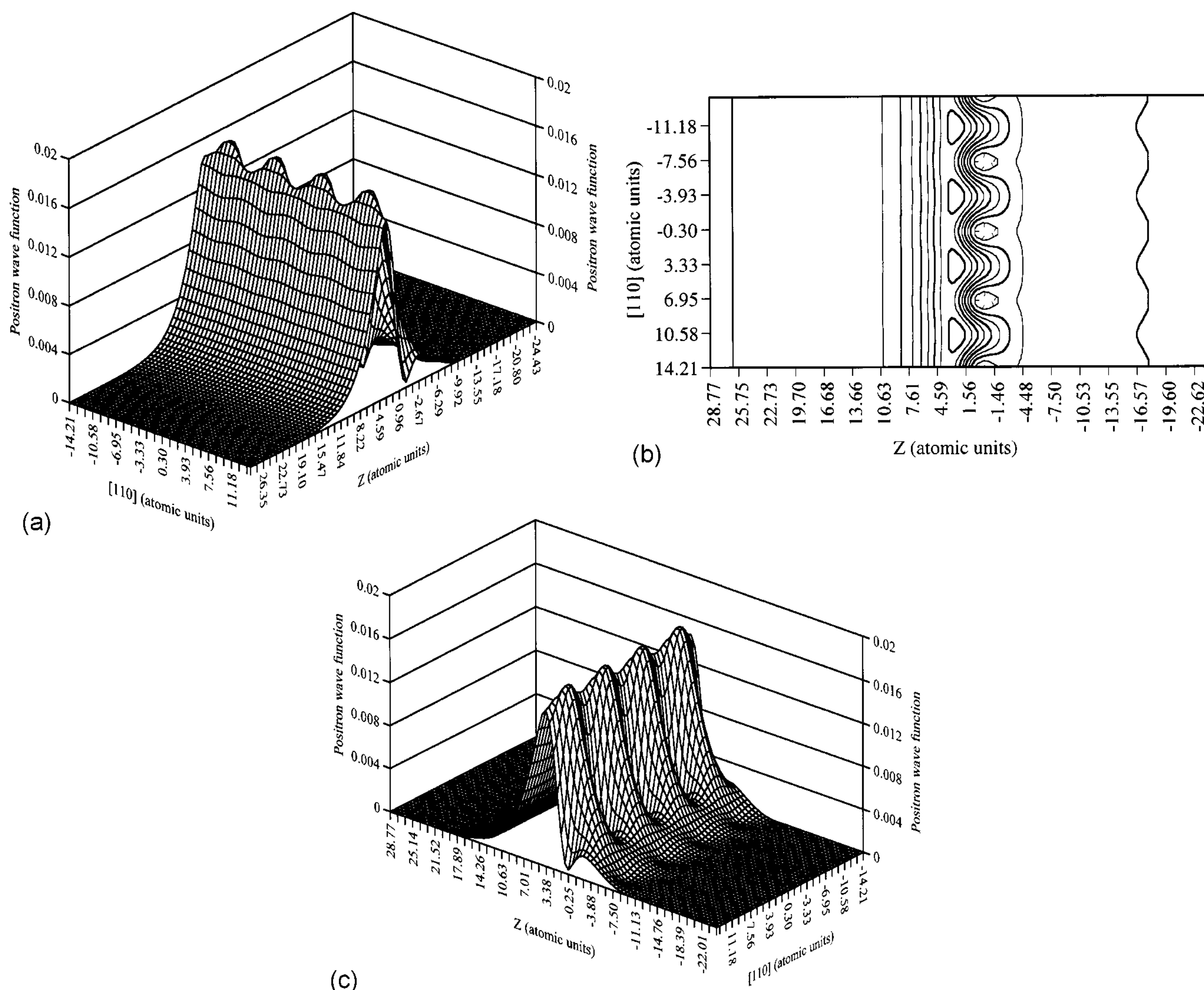

FIG. 3. Calculated ground state wave function for a positron at the clean non-reconstructed Si(100) surface. A: 3D plot (viewed from the vacuum side) for $Y^*=0$. B: Contour plot in the X^*-Z plane for $Y^*=0$ displayed with the vacuum on the left. The contour spacing is 0.0019 atomic units. C: 3D plot (viewed from the bulk) for $Y^*=0$.

obtained for E_b^{theor} also show that the binding energy of the surface trapped positron at the Si(100) surface decreases with the reconstruction due to the decrease in the total electron density at the topmost layer of surface atoms with the reconstruction.

C. Positrons at the reconstructed Si(111)-(7×7) surface

The (7×7) reconstruction of the Si(111) surface is described within the dimer-adatom-stacking fault (DAS) model[48] within which each (7×7) supercell consists of 12 atoms in the adatom layer, 42 atoms in the restatom layer, and 48 atoms in the layer containing the stacking fault, while all layers below are complete. We use positions of Si atoms of the reconstructed Si(111)-(7×7) surface within the DAS model that were determined from low-energy electron diffraction (LEED) measurements.[49] The surface atoms are laterally and vertically displaced by up to 1.2665 and 0.3781 a.u., respectively from the positions evaluated from the transmission electron diffraction (TED) data. The adatoms are relaxed inward by ~0.3781 a.u. and the bond lengths to their nearest neighbors amount to 4.4405 a.u. that is shorter by 0.1% than the bulk bond length. The atoms in the second layer below the adatoms are depressed inward by 1.1342 a.u. and the bonds to the three neighbors in the first layer are stretched by 1.4% on the average compared with the bulk bond length while the distance to the atom beneath in the third layer is shortened by 8.34% with regard to the bulk value. The dimers in the first layer exhibit a bond length of 4.6314 a.u., and are thus elongated by 4.3% with regard to the bulk bond length. The positions of the lower lying Si atoms are taken to correspond to their positions for the ideal Si lattice.

The outermost plane of Si atoms is taken to reside at $Z=0$. The effective image-plane position Z_0 is determined to be 2.73 a.u. from the top layer of atoms along a line normal to the surface and going through a reference atom. The positron surface state calculations for the clean reconstructed Si(111)-(7×7) surface are performed with $\Delta V=3.5$ eV, the

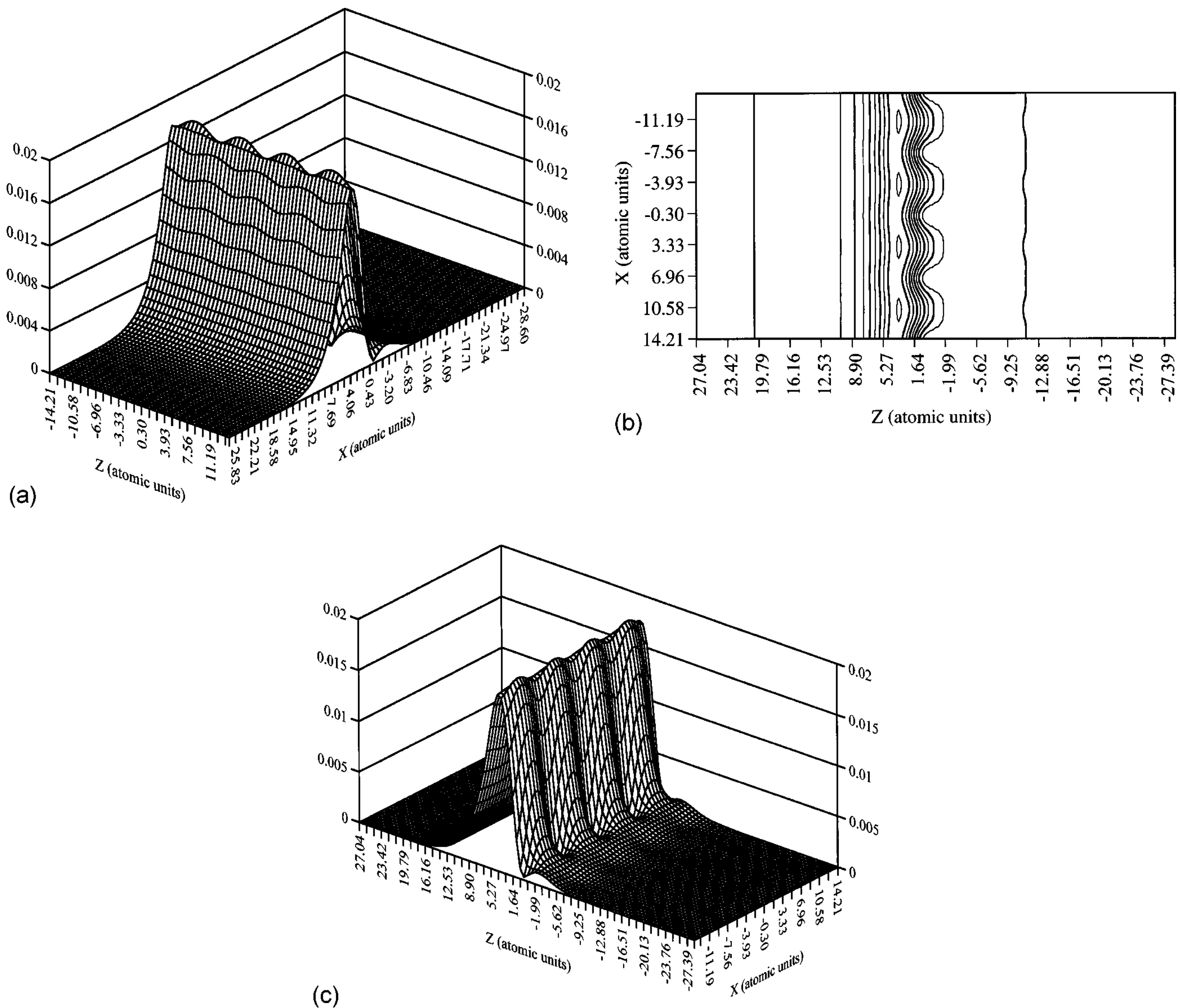

FIG. 4. Calculated ground state wave function for a positron at the clean non-reconstructed Si(111) surface. A: 3D plot (viewed from the vacuum side) for $Y=0$. B: Contour plot in the $X-Z$ plane for $Y=0$ displayed with the vacuum on the left. The contour spacing is 0.002 atomic units. C: 3D plot (viewed from the bulk) for $Y=0$.

value for the height of the ramp potential that provides the best agreement for the ground state energy in the bulk with the experimental positron work function $\Phi_{+}=0$ eV for the reconstructed Si(111)-(7×7) surface[37] (see Table I). Scanning tunneling microscope (STM) and photoelectron spectroscopies have detected three electron surface states, S_1, S_2, and S_3, that appear at about 0.2, 0.8, and 1.8 eV below the Fermi level, respectively.[42,45,50] The S_1 and S_2 surface states are associated with the dangling bonds on the adatoms and restatoms, respectively, while the S_3 surface state is associated with the back bonds of the adatoms.[42,45,50] Since the energy of the S_2 state is lower than the energy of the S_1 surface state, electrons are transferred from the adatoms to the restatoms, thus giving rise to a charge transfer from the adatoms to the restatoms of the (7×7) mesh. Following these surface charge rearrangements, the position of z_1 is chosen to coincide with the plane of the rest atoms and z_2 is set equal to half of the interlayer distance.

Plots of the positron potential and the ground state positron wave function are presented in Figs. 9 and 10. It may be seen in these plots that the positron potential at the reconstructed Si(111)-(7×7) surface contains deep corrugations extending through the topmost layer into the bulk in the region of the corner holes, where Si atoms are substantially displaced from their ideal terminated positions due to the (7×7) reconstruction. These corrugations are even deeper than corrugations seen at the reconstructed the Si(100) -(2×1) surface. Such deep corrugations are notably absent at the non-reconstructed Si and transition metal surfaces. These corrugations of the positron potential at the Si(111) -(7×7) surface define a wide and deep *3d* potential well with a minimum in the center of corner holes. Comparison of the plots in Figs. 3, 4, 6, 8, and 10 shows that the (7×7) reconstruction of the Si(111) surface causes more dramatic changes in the behavior and localization of the positron surface state wave function when compared to the non-

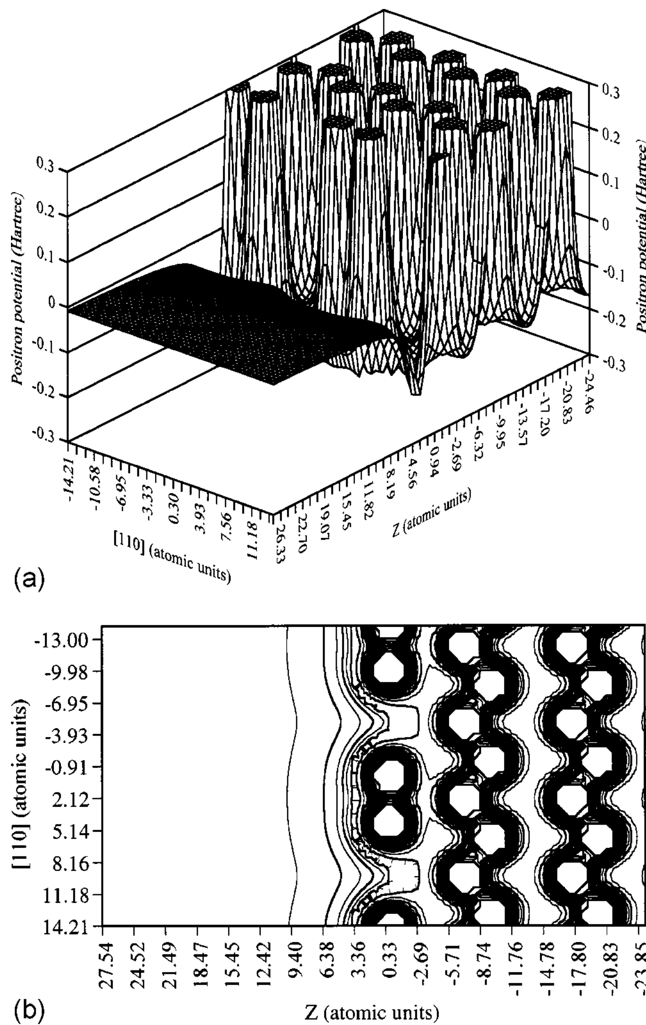

FIG. 5. Calculated potential for a positron at the clean reconstructed Si(100)-(2×1) surface described within the symmetric dimer model. A: 3D plot (viewed from the vacuum side) for $Y^*=0$. B: Contour plot in the X^*-Z plane for $Y^*=0$ displayed with the vacuum on the left. Contours are separated by 0.042 Hartree.

reconstructed surface than the (2×1) reconstruction of Si(100) surface. The width and depth of the potential well at the corner holes of the reconstructed Si(111) -(7×7) surface result in the positron surface state wave function being almost completely localized in all three dimensions within the well, with a maximum in the center of the corner hole regions 1.95 a.u. below the topmost atomic layer of the (111) surface with the (7×7) reconstruction. The modulus of the positron surface state wave function decreases from its maximum value by factors of 22 and 144 about 12 and 20 a.u. away from the center of the corner hole, respectively, in the X and Y directions. Comparison of Figs. 4 and 10 also shows that the localization of the positron surface state wave function in the corner hole regions of the reconstructed Si(111)-(7×7) surface results in a significant decrease in the overlap of the positron surface state wave function with core-level electrons of Si atoms at the surface.

The *3d* trapping of positrons had previously been put forward in Ref. 37 as one possible explanation for the essentially isotropic electron-positron pair momentum density observed in the studies of positron interactions with the reconstructed Si(111)-(7×7) surface using the technique of two-dimensional angular correlation of annihilation radiation (2D-ACAR). Our results indicating the localization of the positron surface state wave function in all three dimensions in the corner hole regions of the reconstructed Si(111)-(7×7) surface serve as a theoretical demonstration of such *3d* trapping of positrons and lend strong credence to such localization as the correct explanation of the experimental observations.

The computed binding energy of a positron trapped at the reconstructed Si(111)-(7×7) surface described within the DOS model converge to $E_b^{\rm theor}=2.70$ eV, which agrees well with the experimental value of the positron binding energy for this surface, $E_b^{\rm exper}=2.69(7)$ eV.[5,40] Similar to the case of the reconstructed Si(100)-(2×1) surface, $E_b^{\rm theor}$ for the positron trapped at the reconstructed Si(111)-(7×7) surface exceeds the positron work function for the bulk Si terminated with the reconstructed Si(111)-(7×7) surface. Thus, the calculated positron surface state is the ground state at this reconstructed surface.

The calculated value for the positron binding energy is comparable to E_b for the positrons trapped at the Cu(100) and Cu(111) surfaces, 2.77(5) and 2.80(5) eV, respectively.[15,16,18] However the positron surface state wave functions are quite different at these surfaces due to the larger in-plane variations of the potential well at the Si surface in comparison to the "*quasi-1d*" well at the Cu surfaces. Other contributing factors are the lower total electron density in Si as compared to the transition metal, differences in electron-positron correlations in the transition metal and the elemental semiconductor, and a change in the position of the image surface due to the (7×7) reconstruction of the Si(111) surface. The measured positron work functions $\Phi_+^{\rm exper}$ are also comparable: ~0.0, –0.3(2), and –0.4(2) eV for the Si(111), Cu(100), and Cu(111) surfaces,[37,51] respectively. Thus, the energy difference between the surface and bulk states ΔE, obtained for the reconstructed Si(111)-(7×7) surface, is comparable to ΔE for the (100) and (111) surfaces of Cu. However the extent to which the positron surface state wave function penetrates into the bulk Si terminated by the reconstructed Si(111)-(7×7) surface is quite different than the one observed for the transition metal surfaces due to the localization of the positron surface state wave function in all three dimensions at the corner hole regions.

The results obtained for $E_b^{\rm theor}$ also show that the binding energy of the surface trapped positron increases with the (7×7) reconstruction due to a wider and deeper *3d* potential well at the corner holes of the reconstructed Si(111) -(7×7) surface when compared to the "*quasi-1d*" potential well at the non-reconstructed Si(111) surface. Thus, the largest values of the positron binding energy E_b are correlated with the surfaces of smallest atomic density.

IV. POSITRON ANNIHILATION CHARACTERISTICS

Calculations of the annihilation rate of the surface trapped positron, λ (the inverse of the positron surface state lifetime,

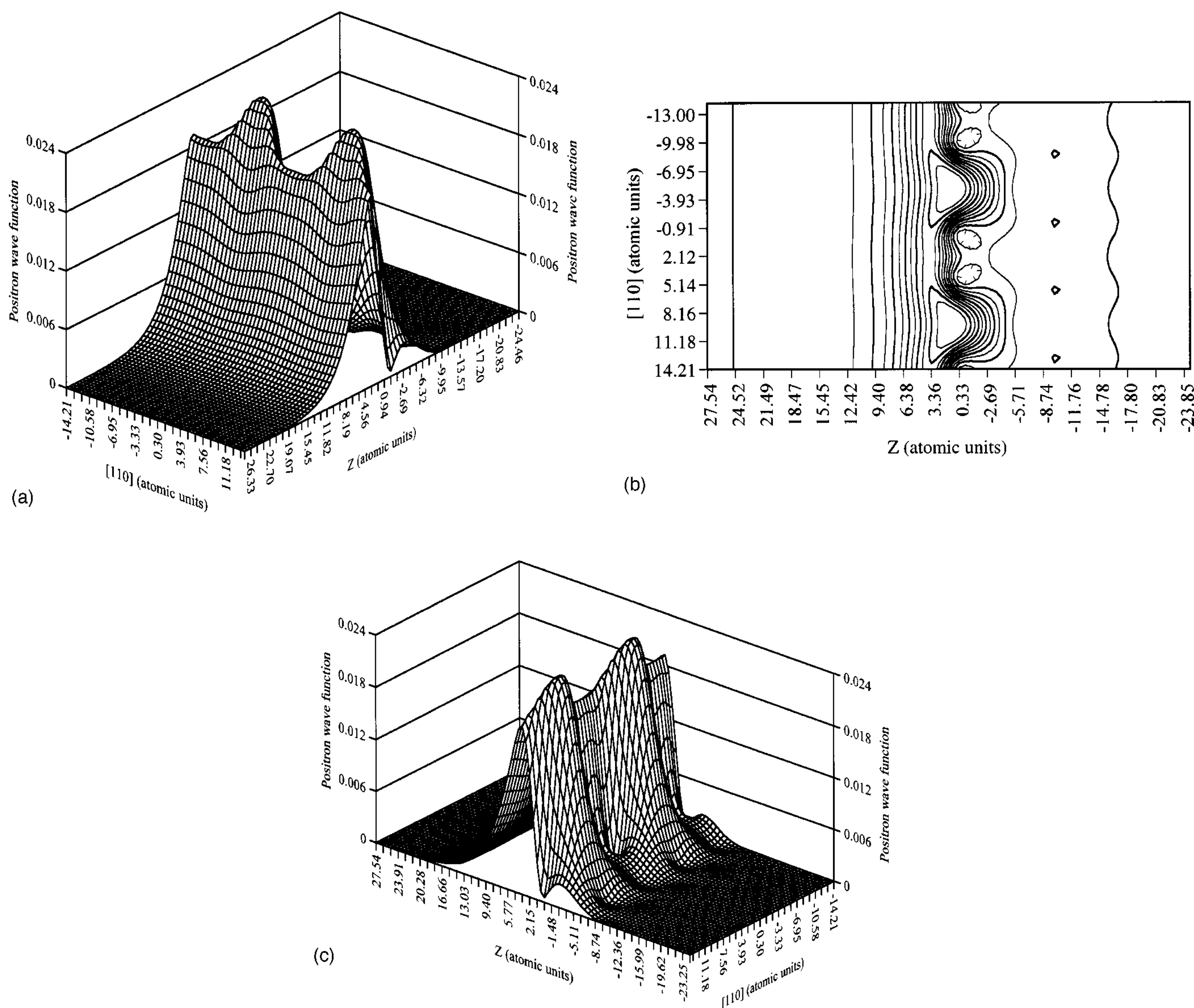

FIG. 6. Calculated ground state wave function for a positron at the clean reconstructed Si(100)-(2×1) surface described within the symmetric dimer model. A: 3D plot (viewed from the vacuum side) for $Y^*=0$. B: Contour plot in the X^*-Z plane for $Y^*=0$ displayed with the vacuum on the left. The contour spacing is 0.002 atomic units. C: 3D plot (viewed from the bulk) for $Y^*=0$.

τ_s) are performed taking electron-positron correlation effects explicitly into account by using a formalism based on the local density approximation (LDA). The expression for λ within the LDA may be expressed as[33]

$$\lambda = \frac{\pi r_o^2 c}{e^2} \int d^3\boldsymbol{r} n^+(\boldsymbol{r}) n_-(\boldsymbol{r}) \Gamma[n_-(\boldsymbol{r})], \qquad (10)$$

where r_o is the classical electron radius, c is the speed of light, $n^+(\boldsymbol{r})$ is the positron charge density, $n(\boldsymbol{r})$ is the electron charge density, and $\Gamma[n_-(\boldsymbol{r})]$ is the short-range annihilation enhancement factor in an electron gas of density $n_-(\boldsymbol{r})$, which takes account of the fact that the electrons are attracted toward the positively charged positron, increasing the overlap of the positron and the electron wave functions and hence the annihilation rate. Outside the semiconductor surface, the LDA breaks down due to the fact that the correlation component of the positron potential is no longer related to the electron density at the position of the positron, but is due to the presence of the semiconductor surface with accumulated electrons on it. Following Ref. 52, we modify the LDA result for λ by assuming the enhancement factor $\Gamma[n_-(\boldsymbol{r})]$ to be nonzero for all $\boldsymbol{r}$ inside the bulk region, and to be zero for all $\boldsymbol{r}$ inside the image potential region.

Due to the existence of the band gap, the valence electrons do not respond to external perturbations as effectively as do the conduction electrons in metals. As a result, the positron screening in semiconductors is not as effective as in metals. This is taken into account in our calculations of the total annihilation rate by using the following modified interpolation form for the enhancement factor $\Gamma[n_-(\boldsymbol{r})]$, suggested by Puska[52] on the basis of the many-body calculations[33,53]

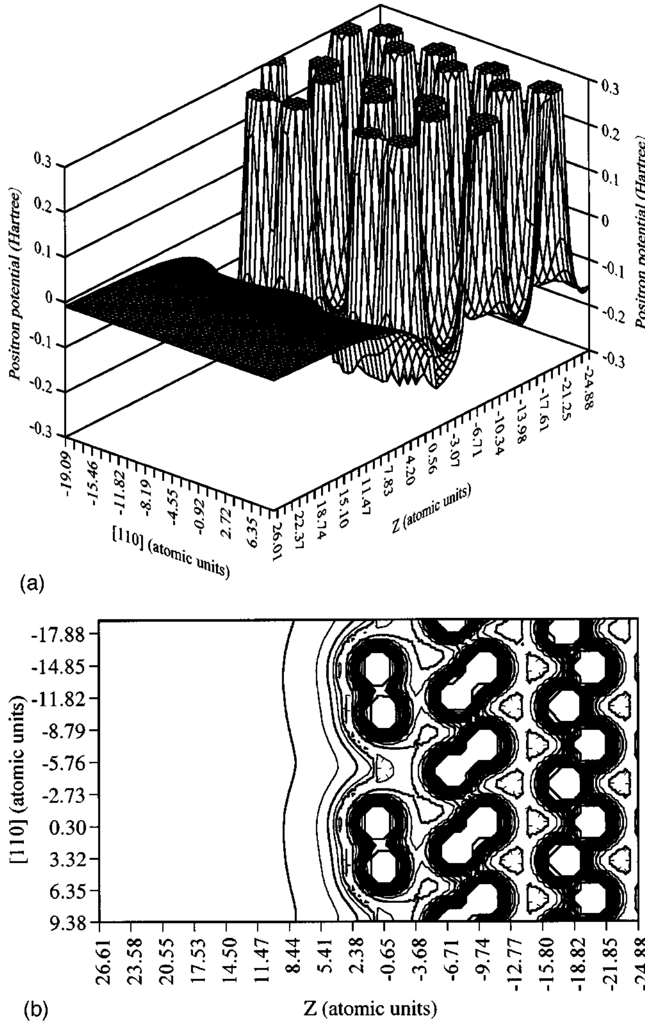

FIG. 7. Calculated potential for a positron at the clean reconstructed Si(100)-(2×1) surface described within the asymmetric dimer model. A: 3D plot (viewed from the vacuum side) for $Y^*=0$. B: Contour plot in the X^*-Z plane for $Y^*=0$ displayed with the vacuum on the left. Contours are separated by 0.035 Hartree.

$$\Gamma_{\mathrm{LDA}}[n_-(\boldsymbol{r})] = 1 + 1.23r_s + 0.8295r_s^{3/2} - 1.26r_s^2 + 0.3286r_s^{5/2} + (1 - 1/\varepsilon_\infty)r_s^3/6, \tag{11}$$

where r_s is the usual electron density parameter of a homogeneous electron gas, $[(4\pi/3)r_s^3 n_- = 1]$, and ε_∞ is the high-frequency dielectric constant. The form of Eq. (11) is justified by two constraints for the screening cloud of the positron given by Eqs. (5a) and (5b).[32,52]

The results of calculations of the surface state lifetime τ_s for a positron trapped at the Si(100) and Si(111) surfaces and of the positron bulk state lifetime τ_B for bulk Si terminated by the (100) and (111) surfaces are presented in Table II.

The positron annihilation rate $\lambda_{n,l}$ with specific core-level electrons, described by quantum numbers n and l, is computed within the LDA from the overlap of positron and electron densities using Eq. (12):

$$\lambda_{n,l} = \pi r_o^2 c \int d^3\boldsymbol{r}\, \gamma(\boldsymbol{r}) |\psi^+(\boldsymbol{r})|^2 \left[\sum_i |\psi_{n,l}^i(\boldsymbol{r})|^2 \right], \tag{12}$$

where $\gamma(\boldsymbol{r})$ is a local enhancement factor to account for the electron-positron correlation effects[54,55] that increase the positron annihilation rate, Ψ^+ is the positron wave function, $\Psi_{n,l}^i$ is the wave function of the core electron described by quantum numbers n and l. We use for $\gamma(\boldsymbol{r})$ the interpolation form given in Ref. 52. The summation in Eq. (12) is performed over all electrons in the atomic level defined by quantum numbers n and l. The core annihilation probabilities $\rho_{n,l}$ with the specific core electron shells can be obtained by dividing the partial positron annihilation rate $\lambda_{n,l}$ with the different core shells by the total positron annihilation rate λ, i.e., $\rho_{n,l}=\lambda_{n,l}/\lambda$. The computed values of the positron annihilation probabilities, $p_{n,l}$, with Si $2s$ and $2p$ core-level electrons for the non-reconstructed and reconstructed Si(100) and Si(111) surfaces are presented in Table III.

We can deduce the following important facts from the computed values of the positron surface state lifetimes τ_s presented in Table II. First, the values of τ_s computed for all Si surfaces studied are considerably larger than the bulk Si lifetime τ_B, as expected. Second, like the positron binding energy, the calculated positron surface state lifetime τ_s is found to be sensitive to reconstruction and atomic composition of the top layers of the Si(100) and Si(111) surfaces. The computed values of τ_s are equal to 687 ps for the reconstructed Si(100)-(2×1) surface, described within asymmetric dimer model, and 484 ps for the reconstructed Si(111) -(7×7) surface, respectively. The large difference in calculated surface state lifetimes for these two surfaces indicate that surface state lifetime measurements could be used to probe surfaces of different reconstructions. Third, the computed positron bulk lifetime, τ_B^{theor}, for bulk Si terminated by the (100) and (111) surfaces is found to be in good agreement with the experimental bulk Si lifetime, τ_B^{exper}. This supports the fact that the positron potential used in our calculations provides a good approximation to the actual potential experienced by the positron in the bulk semiconductor.

It can be seen in Table III that the theoretical annihilation probabilities of the surface trapped positrons with Si $2s$ and $2p$ core-level electrons are significantly different for the two reconstructed Si surfaces studied. For example, the Si $2p$ core annihilation probability changes from 1.86% for the reconstructed Si(100)-(2×1) surface, described by the symmetric dimer model, to 0.49% for the reconstructed Si(111) -(7×7) surface.

The different values for the Si $2s$- and $2p$-core annihilation probabilities obtained for (100) and (111) surfaces of Si with (2×1) and (7×7) reconstructions reflect differences in the localization of the positron surface state wave function at these surfaces and show the sensitivity of positron annihilation characteristics to a specific atomic structure of the topmost layers of a semiconductor. It should be noted that metal surfaces showed little variation of positron annihilation characteristics for different surfaces of the same metal.[7,10–12,18] The increased sensitivity of the positron surface state wave function to the reconstructions in semiconductors reflects the

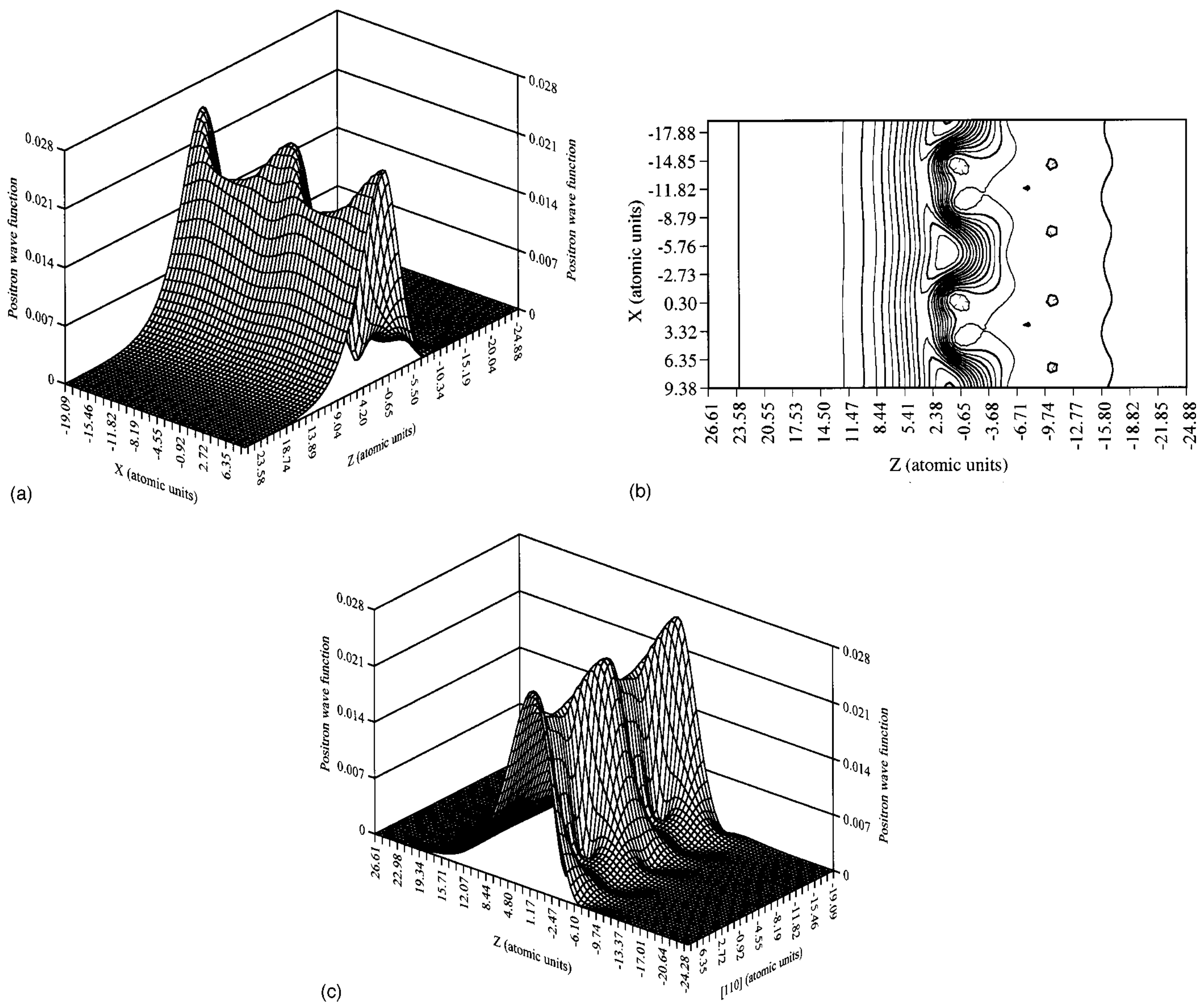

FIG. 8. Calculated ground state wave function for a positron at the clean reconstructed Si(100)-(2×1) surface described within the asymmetric dimer model. A: 3D plot (viewed from the vacuum side) for $Y^*=0$. B: Contour plot in the X^*-Z plane for $Y^*=0$ displayed with the vacuum on the left. The contour spacing is 0.001 75 atomic units. C: 3D plot (viewed from the bulk) for $Y^*=0$.

fact that reconstructions at the relatively open semiconductor surfaces produce much larger changes in electron densities (and the resulting positron surface potentials) than do the more moderate reconstructions at the close-packed transition-metal surfaces. The smaller value of the Si *2s* and *2p* core electron annihilation probabilities obtained for the Si(111)-(7×7) surface when compared to the ones obtained for the Si(100)-(2×1) surface reflects significant differences in the behavior of the positron surface state wave function at both surfaces. In particular, the presence of relatively large "corner holes" on the reconstructed Si(111)-(7×7) surface causes localization in all three dimensions of the positron surface state wave function in these regions, thus, significantly reducing the overlap of the positron surface state wave function with core electrons of Si atoms at the reconstructed Si(111)-(7×7) surface when compared with the one that takes place at the Si(100) surface with the (2×1) reconstruction.

In order to properly compare theoretical and experimental core annihilation probabilities, consideration must be given to the Auger transition branching ratios for the various Auger transitions which may result following the formation of a given core hole. In particular, the majority of *3s* holes decay through the $L_1L_{2,3}V$ Auger channel leaving a hole in the *2p* shell, which results in subsequent $L_{2,3}VV$ Auger emission. Taking into consideration the Auger branching ratios for different decay channels of the core holes from Ref. 58 the probabilities of the surface-trapped positrons giving rise to $L_{2,3}VV$ Auger electrons are found to be 2.49% and 2.37% for the reconstructed Si(100)-(2×1) surface, described within symmetric and asymmetric dimer models, respectively, and 0.66% for the reconstructed Si(100)-(7×7) surface, described within the DAS model.

It should be noted that these results agree well with the experimental positron annihilation probabilities with Si core-level electrons obtained from estimates of the intensities of

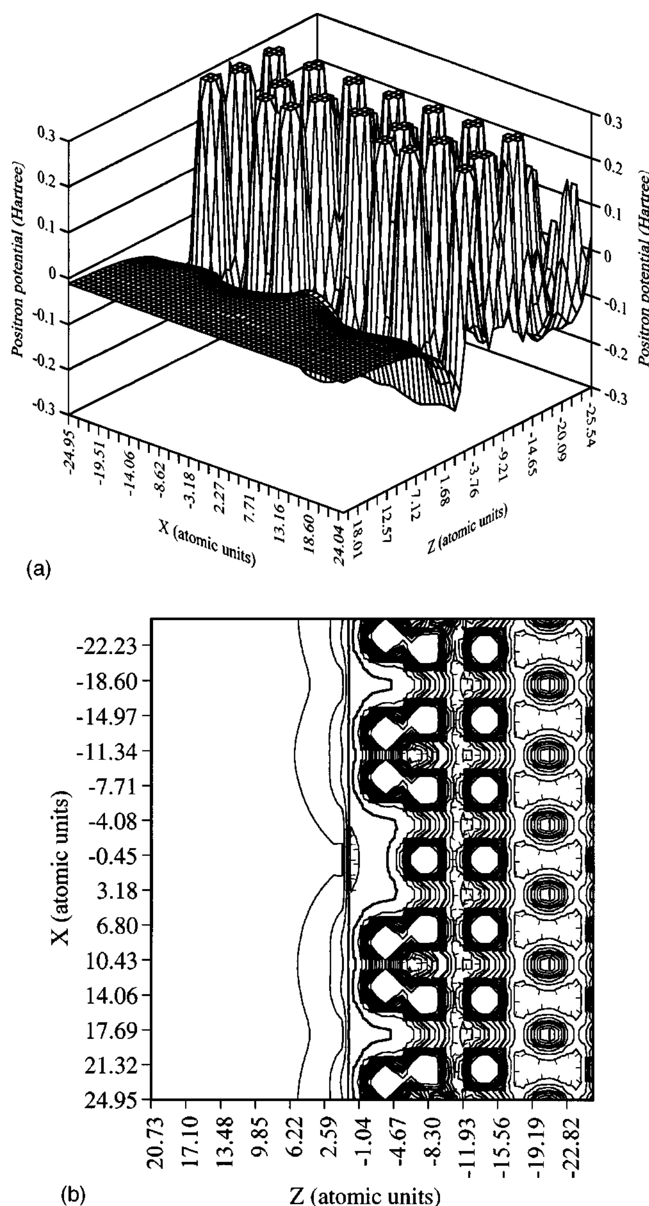

FIG. 9. Calculated potential for a positron at the clean reconstructed Si(111)-(7×7) surface. A: 3D plot (viewed from the vacuum side) for $Y=0$. B: Contour plot in the X–Z plane for $Y=0$ displayed with the vacuum on the left. Contours are separated by 0.045 Hartree.

the positron annihilation induced $L_{2,3}VV$ Auger transitions: 2.01(2)% and 0.65(1)% for reconstructed Si(100)-(2×1) and Si(111)-(7×7) surfaces, respectively.[17] The best agreement with experimental data[5,17] is achieved for the reconstructed Si(100)-(2×1) surface described within the asymmetric dimer model. The $3d$ trapping of the positron in the corner hole regions of the reconstructed Si(111)-(7×7) surface results in a reduced overlap of the positron surface state wave function with the core electrons of the neighboring Si atoms. This explains the reduction in the Si $2s$- and $2p$-core annihilation probabilities when compared to the results for the Si(100)-(2×1) surface.

The computed probabilities of annihilation for the surface trapped positron with Si core-level electrons for both semiconductor surfaces are smaller than the ones obtained from PAES measurements on transition metal surfaces[16] [e.g., 8.70% for Cu(100) and 3.39% for Fe(100), and 8.02% for Pd(100)]. These results for Si surfaces are consistent with the fact that the probability of annihilation of the surface trapped positrons with electrons of the deeper core levels of atoms should be smaller than with electrons of the outer ones due to repulsion of the positron by the nucleus.

The values chosen for the position of the effective image-potential plane Z_0, the height of the ramp potential ΔV, and the positions of the start and the end of the ramp potential, z_1, and z_2, respectively, can be justified theoretically (see Sec. III), and result in calculated values of the positron surface binding energy in good agreement with measured values. To test the sensitivity of the core annihilation probabilities to the specific choice of these parameters, we performed the calculations having modified these parameters. The positions of the start and the end of the ramp potential, z_1, and z_2, respectively, were changed up to 1.5 a.u.; in particular, the end of the ramp potential z_2 was also chosen to coincide with the topmost layer of atoms for both Si surfaces. The height of the ramp potential ΔV was changed by 0.15 eV. The position of the effective image-potential plane Z_0 was changed by 0.3 a.u. The test calculations performed for all studied Si surfaces have shown that these modifications of Z_0, ΔV, z_1, and z_2 have a very small effect on localization and spatial extent of the positron surface states at semiconductor surfaces. These modifications of ΔV, z_1, and z_2 were found to cause negligible changes in positron binding energy, the positron surface state lifetime, and in the annihilation probabilities of the surface trapped positrons with Si $2s$- and $2p$-core electrons for both the (100) and (111) surfaces of Si (of the order of 1%–2%, 1%, and less than 1%, respectively). The modifications of Z_0 were found to cause relatively small changes of the order of 10%, 7%, and 15% in the positron binding energy, the positron surface state lifetime, and in the core annihilation probabilities, respectively. The test calculations with modified parameters have shown that the annihilation probabilities of the surface trapped positrons with Si $2s$- and $2p$-core electrons remain significantly smaller for the reconstructed Si(111)-(7×7) surface when compared with the results for the Si(100)-(2×1) surface, in agreement with experimental PAES data.

V. CONCLUSIONS

We have performed theoretical studies of the “image-potential” positron surface states at clean non-reconstructed and reconstructed Si(100)-(2×1) and Si(111)-(7×7) surfaces using a modified superimposed-atom method, which includes discrete-lattice effects to account for the state of reconstruction of the semiconductor surface. The positron has been treated as a single charged particle in a “correlation well” in the proximity of surface atoms. Positron surface states have been calculated by solving the three-dimensional Schrödinger equation numerically using the finite difference relaxation technique.

The positron surface states at all Si surfaces studied were found to have a lower energy than the energy of the lowest

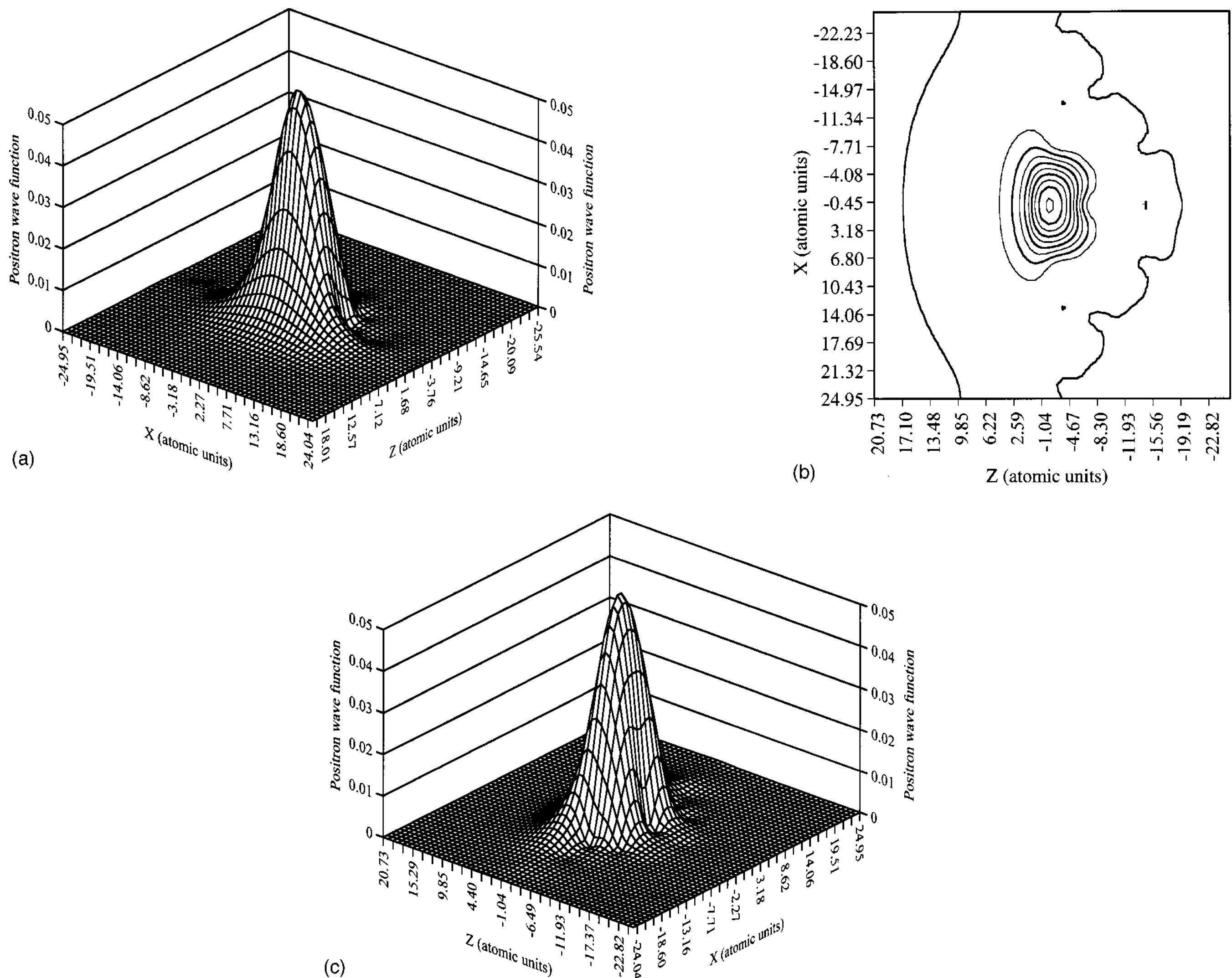

FIG. 10. Calculated ground state wave function for a positron at the clean reconstructed Si(111)-(7×7) surface. A: 3D plot (viewed from the vacuum side) for $Y=0$. B: Contour plot in the $X-Z$ plane for $Y=0$ displayed with the vacuum on the left. The contour spacing is 0.006 atomic units. C: 3D plot (viewed from the bulk) for $Y=0$.

lying extended bulk state indicating that the surface state is a stable trap for the positron prior to annihilation. The positron surface state wave function has been found to be localized mostly in the potential well on the vacuum side at both non-reconstructed Si(100) and Si(111) surfaces. The positron surface state wave function calculated for the reconstructed Si(100)-(2×1) surface, while still localized in the potential well on the vacuum side of the topmost layer of Si atoms, was found to extend through the topmost layer into the Si lattice in the regions where atoms are displaced from their ideal terminated positions due to the (2×1) reconstruction. The positron surface state wave function was found to penetrate even deeper into the Si lattice and to have its maximum shifted even closer to the Si atoms of the topmost layer than in the case of the non-reconstructed Si(100) surface when the (2×1) reconstruction is described using the asymmetric as compared to the symmetric dimer model.

In the case of the reconstructed Si(111)-(7×7) surface, the much larger displacements of the Si atoms from their ideal terminated positions due to the (7×7) reconstruction were shown to cause the positron potential corrugations to extend significantly deeper into Si lattice and to form a wide and deep potential well with a minimum in the center of corner holes. The positron surface state wave function calculated for this reconstruction was found to be localized in all three dimensions at the corner hole regions of the reconstructed Si(111)-(7×7) surface. This "3d trapping" of the positron in the corner hole regions of the reconstructed Si(111)-(7×7) surface provides an explanation of the essentially isotropic electron-positron pair momentum density distribution observed in 2D-ACAR studies of the positron interactions with the reconstructed Si(111)-(7×7) surface.[37]

It has been shown that the orientation-dependent variations of the atomic density and total electron density at the Si(100) and Si(111) surfaces result in a corresponding dependence of the positron surface binding energy E_b. The computed positron surface binding energy E_b^{theor} has been found to change with surface reconstruction and to be sensitive to the specific atomic structure of the topmost layers of surfaces. The largest values of the positron binding energy have

TABLE II. Theoretical and experimental positron surface-state binding energies E_b, positron surface and bulk state lifetimes, τ, for the clean non-reconstructed Si(100) and Si(111) surfaces, the reconstructed Si(100)-(2×1) surfaces described within symmetric and asymmetric dimer models, and the reconstructed Si(111)-(7×7) surface.

System	E_b (eV) Theory	E_b (eV) Experiment	τ_s surface state (ps) Theory	τ_B bulk state (ps) Theory	τ_B bulk state (ps) Experiment
Non-reconstructed Si(100)	2.53		637	218	219[e]
Reconstructed Si(100)-(2×1) symmetric dimer model	2.12	2.06(7)[a]	674	219	219[e]
Reconstructed Si(100)-(2×1) asymmetric dimer model	2.06	2.06(7)[a]	687	219	219[e]
Non-reconstructed Si(111)	3.20		619	215	219[e]
Reconstructed Si(111)-(7×7)	2.74	2.69(7)[a]	484	219	219[e]
Cu(100)	2.77[c,d]	2.77(5)[b]	478[c,d]	109[d]	109[f]
Cu(111)	2.79[c,d]	2.80(5)[b]	502[c,d]	109[d]	109[f]

[a]Reference 5.
[b]Reference 40.
[c]Reference 22.
[d]Reference 23.
[e]Reference 56.
[f]Reference 57.

been found to be correlated with the surfaces of smallest atomic density. Theoretical positron binding energies E_b^{theor} calculated for the reconstructed Si(100)-(2×1) and Si(111)-(7×7) surfaces described within asymmetric dimer and DAS models, respectively, have been found to agree well with experimental E_b^{exper}.

The impact of various surface reconstructions on the positron surface state lifetime τ_s and the annihilation probabilities of the surface trapped positrons with Si *2s* and *2p* core-level electrons has been studied. Theoretical positron bulk lifetimes τ_B^{theor} for bulk Si terminated by the (100) and (111) surfaces have been found to be in good agreement with experimental bulk values, and positron lifetimes in the surface state τ_s have been found to be larger than in the bulk state, as expected. The computed values of τ_s were found to be significantly different for the reconstructed Si(100)-(2×1) and Si(111)-(7×7) surfaces, respectively, indicating that positron lifetime experiments could be used to distinguish the surfaces of elemental semiconductor with different state of reconstruction.

It has been shown that, unlike different surfaces of transition metals, annihilation probabilities of surface trapped positrons with Si *2s*- and *2p*-core-level electrons are significantly smaller for the reconstructed Si(111)-(7×7) surface when compared with the results for the reconstructed Si(100)-(2×1) surface. It has been confirmed that the sig-

TABLE III. Theoretical and experimental positron annihilation probabilities with relevant core electrons, $p_{n,l}$ at the clean Si(100) and Si(111) surfaces.

System	$p_{n,l}$ (%) surface (Theory) Si *2s*	Si *2p*	Si *2s+2p*	$p_{n,l}$ (%) surface (Experiment) Si *2s+2p*
Non-reconstructed Si(100)	0.59	1.72	2.31	
Reconstructed Si(100)-(2×1) symmetric dimer model	0.63	1.86	2.49	2.01(2)[a]
Reconstructed Si(100)-(2×1) asymmetric dimer model	0.60	1.77	2.37	2.01(2)[a]
Non-reconstructed Si(111)	0.36	1.03	1.39	
Reconstructed Si(111)-(7×7) DAS model	0.17	0.49	0.66	0.65(1)[a]
	Cu *3s*	Cu *3p*	Cu *3s+3p*	Cu *3s+3p*
Cu(100)	1.76[b]	6.40[b]	8.16[b]	8.7(7)[c]
Cu(111)	1.47[b]	5.59[b]	7.06[b]	

[a]Reference 17.
[b]References 22 and 23.
[c]Reference 16.

nificantly different values for the Si $2s$- and $2p$-core annihilation probabilities measured for the Si(100) and Si(111) surfaces with the (2×1) and (7×7) reconstructions, respectively, reflect the differences in behavior and extent of the localization of the positron surface state wave function at these surfaces and show the sensitivity of positron annihilation characteristics to a specific atomic structure of the topmost layers of an elemental semiconductor.

Our calculations of the probabilities for the annihilation of surface trapped positrons with Si $2p$ core electrons agree well with the corresponding probabilities estimated from the PAES measurements on Si(100) and Si(111) surfaces. Comparison of theoretical and experimental data confirms that the best agreement is achieved for the reconstructed Si(100)-(2×1) and Si(111)-(7×7) surfaces described within the asymmetric dimer and DAS models, respectively.

Theoretical annihilation probabilities of the surface trapped positrons with relevant Si core-level electrons estimated for the reconstructed Si(100)-(2×1) and Si(111)-(7×7) surfaces have been found to be significantly smaller than the ones obtained for transition-metal surfaces [only 29% and 8%, respectively, of the ones obtained for the Cu(100) surface].

Theoretical results obtained in this paper confirm that PAES intensities, which are proportional to annihilation probabilities of the surface trapped positrons that results in a core hole, are sensitive to the crystal face and surface structure of the elemental semiconductor.

ACKNOWLEDGMENTS

The authors would like to thank A. P. Mills, Jr., K. G. Lynn, R. N. West, D. M. Chen, and R. M. Nieminen for useful and stimulating discussions. This work was supported in part by the National Science Foundation (DMR 9812628) and the Robert A. Welch Foundation.

[1] K. Nagesha and L. Sanche, Phys. Rev. Lett. **81**, 5892 (1998); F. J. Himpsel, Adv. Phys. **32**, 1 (1983); U. Höfer, I. L. Shumay, C. Reuss, U. Thomann, W. Wallauer, and T. Fauster, Science **277**, 1480 (1997).
[2] P. M. Echenique and J. B. Pendry, Prog. Surf. Sci. **32**, 111 (1990); Th. Fauster and W. Steinmann, in *Photonic Probes of Surfaces*, edited by P. Halevi (Elsevier, Amsterdam, 1995), p. 347; R. M. Osgood, Jr., and X. Wang, in *Solid State Physics*, edited by H. Ehrenreich and F. Spaepen (Academic, San Diego, CA, 1997), Vol. 51, p. 1.
[3] C. H. Hodges and M. J. Stott, Solid State Commun. **12**, 1153 (1973); R. M. Nieminen and C. H. Hodges, Phys. Rev. B **18**, 2568 (1978); R. M. Nieminen and M. Manninen, Solid State Commun. **15**, 403 (1974).
[4] R. M. Nieminen and M. J. Puska, Phys. Rev. Lett. **50**, 281 (1983); **53**, 1298 (1984).
[5] A. P. Mills, Jr., Solid State Commun. **31**, 623 (1979).
[6] K. G. Lynn, Phys. Rev. Lett. **43**, 391 (1979).
[7] K. G. Lynn and D. O. Welch, Phys. Rev. B **22**, 99 (1980); K. G. Lynn and H. Lutz, *ibid.* **22**, 4143 (1980).
[8] I. J. Rosenberg, A. H. Weiss, and K. F. Canter, J. Vac. Sci. Technol. **17**, 253 (1980).
[9] A. Weiss, R. Mayer, M. Jibaly, C. Lei, D. Mehl, and K. G. Lynn, Phys. Rev. Lett. **61**, 2245 (1988).
[10] A. R. Koymen, K. H. Lee, D. Mehl, A. Weiss, and K. O. Jensen, Phys. Rev. Lett. **68**, 2378 (1992).
[11] A. R. Koymen, K. H. Lee, G. Yang, K. O. Jensen, and A. H. Weiss, Phys. Rev. B **48**, 2020 (1993).
[12] N. G. Fazleev, J. L. Fry, J. H. Kaiser, A. R. Koymen, K. H. Lee, T. D. Niedzwiecki, and A. Weiss, Phys. Rev. B **49**, 10577 (1994).
[13] D. Mehl, A. R. Koymen, K. O. Jensen, F. Gotwald, and A. Weiss, Phys. Rev. B **41**, 799 (1990).
[14] R. Mayer, A. Schwab, and A. Weiss, Phys. Rev. B **42**, 1881 (1990).
[15] K. H. Lee, A. R. Koymen, D. Mehl, K. O. Jensen, and A. Weiss, Surf. Sci. **264**, 127 (1992).
[16] A. Weiss, Mater. Sci. Forum **105–110**, 511 (1992); Solid State Phenom. **28&29**, 317 (1992/1993); *Positron Spectroscopy of Solids, Proceedings of the International School of Physics "Enrico Fermi,"* edited by A. Dupasquier and A. P. Mills Jr. (IOS, Amsterdam, 1995), p. 259.
[17] N. G. Fazleev, J. Kim, J. L. Fry, and A. H. Weiss, Phys. Rev. B **68**, 245307 (2003).
[18] S. Amdani, A. Eshed, N. Fazleev, and A. Weiss, in *Principles and Applications of Positron and Positronium Chemistry*, edited by Y. C. Jean, P. E. Mallon, and D. M. Schrader (World Scientific, Singapore, 2003), p. 309.
[19] R. M. Nieminen and K. O. Jensen, Phys. Rev. B **38**, 5764 (1988).
[20] N. G. Fazleev, J. L. Fry, K. Kuttler, A. R. Koymen, and A. H. Weiss, Mater. Sci. Forum **175–178**, 153 (1995).
[21] N. G. Fazleev, J. L. Fry, K. Kuttler, A. R. Koymen, and A. H. Weiss, Appl. Surf. Sci. **85**, 26 (1995).
[22] N. G. Fazleev, J. L. Fry, K. Kuttler, A. R. Koymen, and A. H. Weiss, Phys. Rev. B **52**, 5351 (1995).
[23] N. G. Fazleev, J. L. Fry, and A. H. Weiss, Phys. Rev. B **57**, 12506 (1998).
[24] K. H. Lee, A. R. Koymen, D. Mehl, K. O. Jensen, and A. Weiss, Surf. Sci. **264**, 127 (1992).
[25] O. Gunnarsson and B. I. Lundqvist, Phys. Rev. B **13**, 4274 (1976).
[26] D. M. Ceperley and B. J. Adler, Phys. Rev. Lett. **45**, 566 (1980).
[27] F. Herman and S. Skillman, *Atomic Structure Calculations* (Prentice-Hall, New York, 1963).
[28] N. W. Ashcroft and N. D. Mermin, *Solid State Physics* (Holt, Rienhart, and Winston, New York, 1976).
[29] M. J. Puska and C. Corbel, Phys. Rev. B **38**, 9874 (1988).
[30] J. Arponen and E. Pajanne, Ann. Phys. (N.Y.) **121**, 343 (1979).
[31] W. Brandt and J. Reinheimer, Phys. Rev. B **2**, 3104 (1970).
[32] M. J. Puska, S. Mäkinen, M. Manninen, and R. M. Nieminen, Phys. Rev. B **39**, 7666 (1989).
[33] E. Boronski and R. M. Nieminen, Phys. Rev. B **34**, 3820 (1986).
[34] G. E. Kimball and G. H. Shortley, Phys. Rev. **45**, 815 (1934).
[35] N. D. Lang and W. Kohn, Phys. Rev. B **7**, 3541 (1973).

[36] J. A. van Vechten, in *Handbook of Semiconductors*, edited by S. P. Keller (North-Holland, Amsterdam, 1980), Vol. 3; B. R. Nag, *Electron Transport in Compound Semiconductors* (Springer, Heidelberg, 1980).

[37] D. M. Chen, S. Berko, K. G. Lynn, A. P. Mills, L. O. Roellig, and R. N. West (unpublished), D. M. Chen, Ph.D. dissertation, City College, New York, 1987.

[38] C. M. Goringe, D. R. Bowler, and E. Hernández, Rep. Prog. Phys. **60**, 1447 (1997); I. Ivanov, A. Mazur, and J. Pollmann, Surf. Sci. **92**, 365 (1980).

[39] J. A. Appelbaum, G. A. Baraff, and D. R. Hamann, Phys. Rev. B **11**, 3822 (1975).

[40] P. J. Schultz and K. G. Lynn, Rev. Mod. Phys. **60**, 701 (1988).

[41] R. E. Schlier and H. E. Farnsworth, J. Chem. Phys. **30**, 917 (1959); J. D. Levine, Surf. Sci. **34**, 90 (1973).

[42] H. Neddermeyer, Rep. Prog. Phys. **59**, 701 (1996); D. Haneman, *ibid.* **50**, 1045 (1987).

[43] E. Artacho and F. Induráin, Phys. Rev. Lett. **62**, 2491 (1989); J. P. LaFemina, Surf. Sci. Rep. **16**, 137 (1992).

[44] J. A. Appelbaum, G. A. Baraff, and D. R. Hamann, Phys. Rev. B **12**, 5749 (1975); **14**, 588 (1976).

[45] G. V. Hansson and R. I. G. Uhrberg, Surf. Sci. Rep. **9**, 197 (1988); E. Landermark, C. J. Karlsson, Y.-C. Chao, and R. I. G. Uhrberg, Phys. Rev. Lett. **69**, 1588 (1992).

[46] D. J. Chadi, Phys. Rev. Lett. **43**, 43 (1979); J. Vac. Sci. Technol. **16**, 1290 (1979); J. Ihm, M. L. Cohen, and D. J. Chadi, Phys. Rev. B **21**, 4592 (1980).

[47] B. W. Holland, C. B. Duke, and A. Paton, Surf. Sci. **140**, L269 (1984).

[48] K. Takayanagi, Y. Tanishiro, M. Takahashi, and S. Takahashi, J. Vac. Sci. Technol. A **3**, 1502 (1985); Surf. Sci. **164**, 367 (1985).

[49] S. Y. Tong, H. Huang, C. M. Wei, W. E. Packard, F. K. Men, G. Glander, and M. B. Webb, J. Vac. Sci. Technol. A **6**, 615 (1988); H. Huang, S. Y. Tong, W. E. Packard, and M. B. Webb, Phys. Lett. A **130**, 166 (1988).

[50] R. J. Hamers, R. M. Tromp, and J. E. Demuth, Phys. Rev. Lett. **56**, 1972 (1986).

[51] M. Jibaly, E. C. Kellogg, A. Weiss, A. R. Koymen, D. Mehl, and L. Stiborek, Mater. Sci. Forum **105–110**, 1399 (1992); M. Jibaly, A. Weiss, A. R. Koymen, D. Mehl, L. Stiborek, and C. Lei, Phys. Rev. B **44**, 12166 (1991).

[52] M. J. Puska, J. Phys.: Condens. Matter **3**, 3455 (1991).

[53] E. Boronski, R. M. Nieminen, and L. Lantto, Phys. Rev. B **32**, 1377 (1985); L. Lantto, *ibid.* **22**, 1380 (1980).

[54] M. Alatalo, B. Barbiellini, M. Hakala, H. Kauppinen, T. Korhonen, M. J. Puska, K. Saarinen, P. Hautojärvi, and R. M. Nieminen, Phys. Rev. B **54**, 2397 (1996).

[55] E. Bonderup, J. U. Andersen, and D. N. Lowy, Phys. Rev. B **20**, 883 (1979).

[56] S. Dannefaer, P. Mascher, and D. Kerr, Phys. Rev. Lett. **56**, 2195 (1986).

[57] A. P. Mills Jr., in *The Proceedings of the International School of Physics "Enrico Fermi" 1981*, edited by W. Brandt (North-Holland, Amsterdam, 1983), p. 432.

[58] E. J. McGuire, Phys. Rev. A **3**, 587 (1971).